Published in final edited form as:
Neuron. 2011 June 23; 70(6): 1128–1142. doi:10.1016/j.neuron.2011.04.027.

Multiple Forms of Activity-Dependent Competition Refine Hippocampal Circuits In Vivo

Masahiro Yasuda[1], **Erin M. Johnson-Venkatesh**[1], **Helen Zhang**[2], **Jack M. Parent**[2], **Michael A. Sutton**[1,3], and **Hisashi Umemori**[1,4,*]

[1] Molecular & Behavioral Neuroscience Institute, University of Michigan Medical School, Ann Arbor, MI 48109-2200

[2] Department of Neurology, University of Michigan Medical School, Ann Arbor, MI 48109-2200

[3] Department of Molecular and Integrative Physiology, University of Michigan Medical School, Ann Arbor, MI 48109-2200

[4] Department of Biological Chemistry, University of Michigan Medical School, Ann Arbor, MI 48109-2200

SUMMARY

Efficient memory formation relies on the establishment of functional hippocampal circuits. It has been proposed that synaptic connections are refined by neural activity to form functional brain circuitry. However, it is not known whether and how hippocampal connections are refined by neural activity *in vivo*. Using a mouse genetic system in which restricted populations of neurons in the hippocampal circuit are inactivated, we show that inactive axons are eliminated after they develop through a competition with active axons. Remarkably, in the dentate gyrus, which undergoes neurogenesis throughout life, axon refinement is achieved by a competition between mature and young neurons. These results demonstrate that activity-dependent competition plays multiple roles in the establishment of functional memory circuits *in vivo*.

INTRODUCTION

The hippocampus plays a central role in the formation, consolidation and storage of explicit memory (Squire et al., 2004). The hippocampal circuit (Figure 1B) consists of highly organized unidirectional synaptic connections called the trisynaptic pathway: from layer II neurons of the entorhinal cortex (EC) to dentate gyrus (DG) granule cells to CA3 pyramidal cells to CA1 pyramidal cells to EC neurons (Amaral and Witter, 1989; Eichenbaum, 2000; Squire et al., 2004; Witter et al., 1989). The hippocampus contains neurons termed place cells, whose firing rate sharply increases when an animal moves through a particular spatial location in an environment. Thus, the hippocampus is hypothesized to form a cognitive map of an individual's local environment (O'Keefe and Nadel, 1978). Place cells are pyramidal

*To whom correspondence should be addressed. Hisashi Umemori, Molecular & Behavioral Neuroscience Institute and Department of Biological Chemistry, University of Michigan Medical School, Room 5065, BSRB, 109 Zina Pitcher Place, Ann Arbor, MI 48109-2200, Phone: 734-763-5242, Fax: 734-936-2690, umemoh@umich.edu.

SUPPLEMENTAL DATA

Supplemental data include five figures and can be found with this article online.

cells in CA1 and CA3, and granule cells in the DG. Place cell-like firing patterns are also recorded from EC neurons (Fyhn et al., 2004; Hafting et al., 2005). This suggests that the trisynaptic pathway plays a critical role for the formation of a cognitive map and spatial memory. Indeed, disruption of synaptic transmission in particular connections in the trisynaptic pathway in rodents led to impaired memory formation (e.g., CA3-CA1 connections: Brun et al., 2002, Nakazawa et al., 2002, Nakashiba et al., 2008; EC-DG-CA3 connections: McHugh et al., 2007). In addition, synaptic defects in the trisynaptic pathway may be involved in neurological disorders. For example, the earliest pathology of Alzheimer's disease patients, whose first symptom is usually amnesia, is the degeneration of EC neurons (Gomez-Isla et al., 1996). This suggests a critical role for the EC-to-DG connection in this disease (Braak and Braak, 1991; deToledo-Morrell et al., 2004). Therefore, the establishment of appropriate trisynaptic connections is essential for efficient learning and memory formation.

It has been proposed that in order to establish appropriate synaptic connections, neural circuits are refined by neural activity during development. Neural activity has been shown to play important roles in the refinement of synapses in sensory and motor systems (Hashimoto and Kano, 2005; Katz and Shatz, 1996; Lichtman and Colman, 2000; Sanes and Lichtman, 1999; Yu et al., 2004). Synapse refinement was first observed at the neuromuscular junction (reviewed in Jansen and Fladby, 1990), and later, it was found in other regions in the nervous system such as in the visual system and cerebellum (Kantor and Kolodkin, 2003; Lohof et al., 1996; Purves and Lichtman, 1980; Lorenzetto et al., 2009). In each of these cases, target cells are initially innervated by several axons from multiple neurons, but they lose most inputs and ultimately become strongly innervated by relatively few axons. Synapse refinement in the sensory and motor systems is clearly an activity-dependent process (Hashimoto and Kano, 2005; Katz and Shatz, 1996; Lichtman and Colman, 2000; Sanes and Lichtman, 1999). By contrast, it is not clear whether activity-dependent refinement controls the pattern of synaptic connectivity in structures involved in spatial learning and memory, such as the intrinsic circuitry in the mammalian hippocampus. It has been shown that activity blockade during synapse formation decreased functional synaptic inputs in primary hippocampal cultures *in vitro* (Burrone et al., 2002). However, because of a lack of appropriate systems that can manipulate activity of specific neuronal populations in the hippocampus *in vivo*, the mechanisms of activity-dependent synapse refinement in the hippocampus are poorly understood.

Here, to investigate the role of neural activity in the establishment of hippocampal circuits in the mammalian brain, we have developed a mouse genetic system in which restricted populations of neurons in the hippocampal circuit can be inactivated by tetanus toxin light chain (TeTxLC) (Figure 1A). Using this system, we examined whether and how neural activity organizes the memory circuit *in vivo*. We identified two distinct modes of activity-dependent refinement of hippocampal connectivity: we show (1) activity-dependent competition between mature neurons refines EC and CA1 axons and (2) in the DG, which undergoes neurogenesis throughout life, a unique form of competition between mature and young neurons refines DG axons. These results demonstrate that multiple forms of activity-dependent competition play important roles in the establishment of functional memory circuits *in vivo*.

RESULTS

Establishment of a Genetic System to Examine the Role of Activity in the Memory Circuit *In Vivo*

Our aim was to investigate the role of neural activity in the formation and modification of memory circuits in the mammalian brain. For this, we established a transgenic mouse system

(Figure 1A), in which neural activity of specific neuronal populations in the hippocampal circuit (Figure 1B) can be controlled *in vivo*. Two kinds of transgenic mouse lines are used in our system (Mayford et al., 1996): tTA (tetracycline transactivator) lines and tetO lines (Figure 1A). tTA lines express tTA in specific neuronal populations in the memory circuit. The tTA lines we used in this study express tTA in either EC or DG+CA1 neurons. TetO lines express transgenes under the control of the tetracycline operator (tetO). When the two lines are mated, transgenes are induced in tTA-expressing neurons (Figure 1A). To inactivate neurons, we used tetanus toxin light chain (TeTxLC) as a transgene. TeTxLC cleaves the cytoplasmic domain of the synaptic vesicle protein VAMP2/synaptobrevin2 to prevent the fusion of synaptic vesicles in presynaptic terminals (Schiavo et al., 1992; Sweeney et al., 1995; Yu et al., 2004). Inactivated axons can be visualized with co-expressed tau-lacZ (Figures 1A and 1C).

Inactive EC Axons Are Eliminated after They Develop

Using the system we have established (Figure 1A), we first examined the role of activity in the major input pathway from the neocortex to the hippocampus - the connection from the medial EC to the DG (Figure 1B) (Amaral and Witter, 1989; Squire et al., 2004; van Groen et al., 2003). The tTA-EC line we used expresses tTA in 43% of the superficial layer neurons of the medial EC (Yasuda and Mayford, 2006), which send axons to the middle third of the molecular layer of the DG. This mouse was mated with a tetO line that expresses tau-lacZ alone (Yasuda and Mayford, 2006) (EC::tau-lacZ) or a line that expresses tau-lacZ and TeTxLC (Yu et al., 2004) (EC::TeTxLC-tau-lacZ) (Figure 1A). We first verified the inhibition of synaptic transmission in EC::TeTxLC-tau-lacZ mice by recording evoked field excitatory postsynaptic potentials (fEPSPs) in the molecular layer of the DG in acute slices. The input-output curves showed that the fEPSP slope of the EC-DG pathway was decreased in the EC::TeTxLC-tau-lacZ mice relative to control littermates by ~35% at postnatal day 11 (P11) (Figures 1D and 1E), while the fiber volley amplitude, which represents the number of axons, was similar between them (Figure 1D and data not shown). This indicates that synaptic transmission by tTA-expressing neurons in the EC::TeTxLC-tau-lacZ line is effectively inactivated by TeTxLC. We then used these mice to examine the developmental projection of active and inactive EC axons in the EC transgenic lines. Both active (EC::tau-lacZ) and inactive (EC::TeTxLC-tau-lacZ) EC axons reached the DG between P6 and P9, as visualized by lacZ staining, without any aberrant projections (Figure 1F). This result suggests that initial axon projections from the EC to the DG are largely independent of synaptic neurotransmitter release.

In contrast, inactivation of EC axons resulted in their elimination from the DG after they developed. Active EC axons (EC::tau-lacZ) increased in the DG from P12 to P16 (Figures 1F and 1G). However, inactive axons (EC::TeTxLC-tau-lacZ) were quickly eliminated from the DG after P12, and very few remained by P18 (Figures 1F and 1G). This axon elimination was likely initiated by axon retraction (also see Figure 4), because (i) no apparent cell death was detected in the EC at P18 (Figure S1B), and (ii) EC axons were still detected in the presubiculum at P21 (Figure S1C). These results suggest that EC axons are refined after P12 in an activity-dependent manner. In EC::tau-lacZ mice, lacZ intensity decreased between P16 and P21 by ~25% (Figure 1G), suggesting that EC axons are refined during normal development and that the elimination of inactive axons in EC::TeTxLC-tau-lacZ mice reflects an exaggerated instance of normal physiological refinement.

Inactive EC Axons Are Eliminated by Activity-Dependent Competition with Active Axons

Since only 43% of the superficial layer neurons of the medial EC express TeTxLC in EC::TeTxLC-tau-lacZ mice (Yasuda and Mayford, 2006), there are two possible mechanisms for the elimination of inactive axons: (i) inactivity *per se* drives axon

elimination, or (ii) they are eliminated via activity-dependent competition with other active EC neurons. To distinguish between these possibilities, we globally suppressed neural activity of EC axons by injecting the sodium channel blocker tetrodotoxin (TTX) (Burrone et al., 2002; Echegoyen et al., 2007) into the DG of EC::TeTxLC-tau-lacZ mice once a day from P9 and analyzed the elimination of TeTxLC-expressing EC axons at P12, P14 and P16 (4, 6 or 8 days total of TTX injections) (Figure 2A). TTX injections markedly suppressed the elimination of TeTxLC-expressing EC axons between P12 and P16 (Figures 2B and 2C). Therefore, the refinement of EC axons in the DG is mostly achieved by an activity-dependent competition between EC neurons. The result that TTX suppressed the elimination of TeTxLC-expressing axons also implies that TeTxLC induced the elimination of axons mainly by inhibiting local neural activity and not by damaging axons or inducing cell death.

Generation of Two tTA Lines to Examine the Refinement of DG Axons *In Vivo*

To understand spatial differences in activity-dependent refinement of hippocampal circuits, we next examined the role of activity in connections between DG and CA3 (Figure 1B). This connection is unique in the hippocampus because it is continuously renewed/added as a result of neurogenesis in the DG throughout life (Gage, 2000; Lie et al., 2004; Ming and Song, 2005). We generated two tTA-lines that express tTA in dentate granule cells (DGCs). We refer to these two lines as the DG-S (some) and DG-A (all) (Figure 3A; these lines also express tTA in CA1, see Figures 8 and S5). tTA-expressing cells in these lines were identified by mating them with an nls-lacZ reporter line (Mayford et al., 1996) (DG-S::nls-lacZ and DG-A::nls-lacZ; Figure 3A), and the percentage of tTA-positive cells was quantified by staining for β-gal and a mature neuronal marker NeuN (Lie et al., 2004; Ming and Song, 2005) (Figures 3B and 3C). DG-S and DG-A lines differ in the percentage of tTA-expressing mature DGCs: a moderate number of mature DGCs express tTA in the DG-S line (37.1 ± 1.4%), while almost all mature DGCs express tTA in the DG-A line (87.8 ± 4.2%) (Figures 3A–3C). This difference in percentage of tTA-expressing DGCs in the two lines was maintained from P15 to P30 (Figure 3A). All β-gal positive cells were NeuN positive, indicating that only mature neurons express tTA (Figure 3B). When these tTA lines are mated with the TeTxLC-tau-lacZ line (DG-S::TeTxLC-tau-lacZ and DG-A::TeTxLC-tau-lacZ), about 37% of mature DGCs should be inactivated in DG-S::TeTxLC-tau-lacZ, which makes a competitive situation, whereas almost all mature DGCs should be inactivated in DG-A::TeTxLC-tau-lacZ, resulting in a non-competitive situation among mature DGCs. Indeed, input-output curves of evoked synaptic responses showed that the fEPSP slope of the DG-CA3 connections in DG-S::TeTxLC-tau-lacZ and DG-A::TeTxLC-tau-lacZ mice were ~44% and ~80% lower, respectively, than in control mice (Figures 3D and 3E), which is consistent with the percentage of tTA-expressing DG neurons in each transgenic line (Figure 3C). Using these two lines, we examined activity-dependent refinement of DG axons.

Inactive DG Axons Are Retracted Regardless of the Number of DG Mature Neurons That Are Inactivated

In the DG-S::TeTxLC-tau-lacZ line (competitive situation among mature DGCs), TeTxLC-expressing DG axons projected into the stratum lucidum layer of CA3 by P12 (Figure 3F). Thus, similar to EC-to-DG connections, initial axon projections from the DG to CA3 were not dependent on synaptic release. At P20, TeTxLC-expressing DG axons were diminishing from CA3, and at P25 and P30 very few axons were detected (Figure 3F). Therefore, in DG-S::TeTxLC-tau-lacZ mice, inactive DG axons were eliminated between P15 and P25.

In the DG-A::TeTxLC-tau-lacZ line (non-competitive situation among mature DGCs), TeTxLC-expressing DG axons also projected to CA3 by P12 (Figure 3G). Surprisingly, however, they were also eliminated between P15 and P25 (Figure 3G). The rate of inactive

DG axon elimination was not affected by the percentage of mature axons that were inactivated (Figure 3H). This elimination was not just a developmental retraction but was induced by synaptic inactivity, because in DG-A::tau-lacZ mice (no TeTxLC), DG axons were maintained at P25 (Figure 3I; quantification at P15 and P23 is shown in Figure 3J).

To further characterize the inactive axon elimination in DG-A::TeTxLC-tau-lacZ mice, we visualized TeTxLC/tau-lacZ-expressing axons by staining with the antibody to β-gal. Confocal microscopy revealed that at P15, TeTxLC-expressing axons were intact at both the proximal and distal regions (Figure 4A). At P20, the proximal region of TeTxLC-expressing axons appeared still intact (Figure 4B, proximal). However, at the distal region of TeTxLC-expressing axons, there were clear signs of axon retraction: swollen axonal tips (retraction bulbs) and remnants of axons (axosomes) (Figure 4B, distal). These features resemble axon retraction observed during synapse elimination at the neuromuscular junction (Bishop et al., 2004). Without TeTxLC (DG-A::tau-lacZ), the distal region of DG axons remained intact at P23 (Figure 4C).

We further examined the morphology of active and inactive DG axons in DG-A::TeTxLC-tau-lacZ mice by sparsely labeling DG axons with a lipophilic tracer, DiI. Inactive (TeTxLC/tau-lacZ-expressing) axons were identified by staining for β-gal. At P18, active (β-gal-/DiI+) DG axons formed many large mossy fiber boutons with long extensions in CA3 (Figure 4D) (Amaral and Dent, 1981). In contrast, inactive (β-gal+/DiI+) DG axons did not have any large mossy fiber boutons (Figure 4D). These results indicate that synaptic transmission plays an important role for the refinement of mossy fiber synapses and that inactive axons are retracted during development.

Is the elimination of inactive DG axons initiated by the death of DG neurons? To address this question, we injected 5-bromo-2-deoxyuridine (BrdU) into DG-A::TeTxLC-tau-lacZ mice at P7–8 to label newborn dentate granule cells (Kee et al., 2002; Kokoeva et al., 2005) and examined the number of surviving BrdU-positive cells at P15, P20, and P25 (Figure 4E). All the BrdU-labeled neurons became NeuN positive mature neurons by P15 (Figure 4F), consistent with earlier reports showing that DG neurons differentiate very quickly during development (Amaral and Dent, 1981; Hastings and Gould, 1999; also see Figure 7). The total number of BrdU-positive cells in DG-A::TeTxLC-tau-lacZ mice was similar to that in wild type mice at P15 and P20 (Figure 4E). In addition, at P20 there was no apparent increase in the number of DG cells that are positive for activated caspase 3, a marker for apoptosis (Figure S2). Since inactive DG axons were being retracted at P20 (Figure 4B), these results suggest that the retraction was not initiated by DG neuron cell death. After mossy fiber elimination (P25), the number of BrdU-positive cells in DG-A::TeTxLC-tau-lacZ mice was significantly decreased (Figure 4E). Therefore, TeTxLC-expressing inactive DG neurons are eventually eliminated after axon retraction, which explains diminished lacZ signals from the whole hippocampus at P25 and P30 in DG::TeTxLC-tau-lacZ mice (Figures 3F and 3G).

Inactive DG Axons Are Retracted as a Result of Activity-Dependent Competition

The result that TeTxLC-expressing DG axons were eliminated between P15 and P25 in DG-A::TeTxLC-tau-lacZ mice, in which almost all mature DG neurons are inactivated (Figures 3G, 3H, and 4B), implies that either (i) DG axons are refined in CA3 by mechanisms other than activity-dependent competition or (ii) axons of mature DGCs compete with an additional neuronal population. To distinguish these two possibilities, we globally suppressed neural activity by administering TTX into the hippocampus of DG-A::TeTxLC-tau-lacZ mice and examined DG axon elimination. We applied TTX by implanting TTX-containing Elvax (Echegoyen et al., 2007) on the hippocampus at P15 (Figure S3A) and prepared horizontal sections at P23 (8 days total of TTX application). TTX applications

significantly inhibited the elimination of inactive DG axons in DG-A::TeTxLC-tau-lacZ mice (Figure 5B), as quantified in Figure 5C (see Figure S3B for methods). Further quantitative analysis revealed that relative to P15 brains, the staining intensities at P23 were 94% in DG-A::tau-lacZ (no TeTxLC) mice, 27% in PBS-treated DG-A::TeTxLC-tau-lacZ mice, and 70% in TTX-treated DG-A::TeTxLC-tau-lacZ mice (Figure S3C). These results indicate that TTX effectively inhibited the elimination of TeTxLC-expressing DG axons in DG-A::TeTxLC-tau-lacZ mice. Therefore, the elimination of TeTxLC-expressing axons in DG-A::TeTxLC-tau-lacZ mice, in which the vast majority of mature DGCs express the transgene, is largely the outcome of activity-dependent competition.

tTA Is Not Expressed by Young Neurons in the tTA-DG Line

To identify axons that compete with TeTxLC-expressing axons in DG-A::TeTxLC-tau-lacZ mice, we characterized tTA-expressing neurons in the DG-A line. In the subgranular zone (SGZ) of the DG, neurons are continuously generated throughout life (Gage, 2000; Lie et al., 2004; Ming and Song, 2005). In DG-A mice, all tTA-expressing neurons were NeuN-positive mature neurons (Figure 3B) and not Ki67-positive dividing neural progenitors in the SGZ (Kee et al., 2002) (Figure 6A). In addition, almost all doublecortin (DCX)-positive immature neurons located adjacent to the SGZ (Kempermann et al., 2003) or calretinin-positive young DGCs (Brandt et al., 2003; Kempermann et al., 2004; Ming and Song, 2005; Li et al., 2009) failed to express tTA (Figures 6B and 6C; 88.8 ± 0.12% of calretinin-positive DGCs do not express tTA). These results raise the possibility that TeTxLC-expressing axons in DG-A::TeTxLC-tau-lacZ mice, which are of mature DGCs, might be competing with axons of young, DCX/calretinin positive DG neurons during refinement.

Suppression of Neurogenesis Inhibits the Elimination of Inactive DG Axons

To address the possibility that axons of mature DGCs are competing with axons of young neurons during refinement, we suppressed neurogenesis in the DG of DG-A::TeTxLC-tau-lacZ mice by injecting the anti-mitotic reagent cytosine arabinoside (AraC) intracerebroventricularly (Elmer et al., 2004; Kokoeva et al., 2005) or intraperitoneally from P15 to P22 and examined the elimination of TeTxLC-expressing axons. Intraperitoneal AraC injections effectively blocked neurogenesis in the DG as shown by the disappearance of Ki67-positive cells from the DGC layer (Figure S4A) and the decrease in the number of NeuN-negative young neurons in the DGC layer (Figure S4B). As shown in Figures 6D and 6E, AraC injections dramatically inhibited the elimination of TeTxLC-expressing axons in DG-A::TeTxLC-tau-lacZ mice, suggesting that the suppression of neurogenesis inhibits the inactive DG axon elimination.

To further confirm the role of neurogenesis in the refinement of DG axons, we performed a similar experiment using temozolomide (TMZ), a DNA-alkylating agent with fewer side effects than AraC (e.g., Garthe et al., 2009), to suppress neurogenesis. We found that TMZ injections also effectively inhibited the elimination of TeTxLC-expressing DG axons in DG-A::TeTxLC-tau-lacZ mice (Figures 6F and 6G). Relative to P15 brains, the staining intensity at P23 was 75% in TMZ-treated DG-A::tau-lacZ mice (Figures 6G and S3C). In addition, TMZ did not appear to affect the pattern of tau-lacZ protein distribution (Figure S4D). These results further support an important role of neurogenesis in DG axon refinement and suggest that axons of mature DG neurons compete with those of young DG neurons for activity-dependent refinement.

Note that TTX administration did not block neurogenesis (Figure S4C), indicating that the ability of TTX to inhibit inactive DG axon elimination (Figures 5B and 5C) is likely due to global activity suppression and not due to a secondary effect on neurogenesis. Interestingly, neurogenesis was enhanced in the DG of DG-A::TeTxLC-tau-lacZ mice during axon

refinement as reflected by enhanced BrdU uptake (Figure 6H). Staining for doublecortin indicated that neurogenesis was more robust in DG-A::TeTxLC-tau-lacZ than DG-S::TeTxLC-tau-lacZ mice (Figure 6I and 6J), suggesting that the degree of axon competition/elimination has an impact on neurogenesis in the DG.

Axons of Newborn Dentate Granule Cells Quickly Form Synapses in CA3 during Refinement

Suppressing neurogenesis from P15 to P22 efficiently inhibited the elimination of inactive DG axons (Figures 6D-G and S3C). This implies that axons of DGCs born between P15 and P22 effectively compete with those of mature DGCs for refinement. If so, newborn DGCs should promptly form synapses in CA3 during refinement. To test this idea, we injected retrovirus that expresses GFP into the DG (Kron et al., 2010) of wild type mice at P15 to label dividing DGC progenitors and examined whether they send axons and form synapses in CA3 by P23 (Figure 7). We found that at P23, i) the axons of DGCs born at P15 elongated through CA3 and reached the border between CA3 and CA1/2 (Figure 7A), ii) the axons formed numerous boutons (~20 per axon), even at the most distal regions of CA3 (Figures 7A and 7B), and iii) these boutons colocalized with presynaptic markers, VGLUT1 and bassoon (Figure 7C). These results indicate that the axons of DGCs born at P15 are synaptically integrated by P23 to compete with mature axons.

AraC Does Not Inhibit the Elimination of Inactive CA1 Axons

To examine the specificity of the effect of AraC, we used DG-S mice. In DG-S mice, tTA is expressed by mature DGCs (37.1 ± 1.4%; Figures 3B and 3C) and CA1 neurons (48.2 ± 3.3%; Figure S5). Using DG-S::TeTxLC-tau-lacZ mice, we addressed whether AraC specifically inhibits the elimination of inactive DG axons or also affects the elimination of inactive CA1 axons. If the effect of AraC is through the suppression of neurogenesis, the elimination of inactive CA1 axons should not be affected. In DG-S::TeTxLC-tau-lacZ mice, axons of TeTxLC-expressing DG and CA1 neurons were both eliminated between P15 and P25 (Figures 3F and 8A). After P25, very few TeTxLC-expressing axons were observed in both regions. On the other hand, DG-S::tau-lacZ mice (no TeTxLC) maintained β-gal-expressing axons of DG and CA1 neurons at P25 (Figure 8C). Thus, in DG-S mice, DG and CA1 axons are refined in an activity-dependent manner between P15 and P25. We administered AraC daily (ip) from P15 to P22 (8 days total) into DG-S::TeTxLC-tau-lacZ mice. AraC injections inhibited the elimination of TeTxLC-expressing DG axons but not that of TeTxLC-expressing CA1 axons (Figure 8D). Therefore, the effect of AraC is specific to DG axons, which is consistent with the fact that neurogenesis is specific to the DG in the hippocampus.

Activity-Dependent Competition of DG Axons Is between Axons of Mature and Young Neurons

Finally, using DG-S mice, we addressed whether the DG axon refinement is mainly achieved by competition between mature and young DG axons or also by competition between mature and mature axons. In DG-S mice, tTA is expressed only by 37.1 ± 1.4% of mature DGCs (Figures 3B and 3C). If competition between mature and mature neurons equally contributes to refinement, AraC injections should not inhibit inactive axon elimination in the DG-S::TeTxLC-tau-lacZ line, which contains both active and inactive mature DGCs. Interestingly however, AraC injections (from P15 to P22) inhibited the elimination of TeTxLC-expressing DG axons in DG-S::TeTxLC-tau-lacZ mice (Figures 8D and 8E) as effectively as in DG-A::TeTxLC-tau-lacZ mice (Figures 6D and 6E). This suggests that the activity-dependent competition of DG axons is largely between axons of mature and young neurons.

To further confirm that young neurons drive inactive axon elimination in the DG, we utilized nestin-tk animals, in which herpes simplex virus thymidine kinase is expressed under the control of the nestin enhancer to drive expression in neural progenitors (Singer et al., 2009). In this animal, administration of ganciclovir efficiently and specifically kills neural progenitors. We mated nestin-tk mice with DG-S::TeTxLC-tau-lacZ mice, injected ganciclovir from P15 to P22, and analyzed their hippocampus at P23. As shown in Figures 8F and 8G, conditional ablation of neurogenesis almost completely blocked (~92%) the elimination of TeTxLC-expressing inactive axons, indicating that competitive refinement of DG axons is preferentially driven by young DG axons.

Together, these results strongly support the conclusion that activity-dependent competition in the DG mainly occurs between mature and young DGCs during postnatal development *in vivo*. Hence, while synapse refinement in different hippocampal subregions involves activity-dependent competition, distinct mechanisms are utilized in different regions.

DISCUSSION

Activity-Dependent Refinement of Memory Circuits *In Vivo*

Neural activity has been shown to play important roles in the formation and refinement of efficient circuits in the sensory-motor systems and in the cerebellum (Buffelli et al., 2003; Hashimoto and Kano, 2005; Hua et al., 2005; Katz and Shatz, 1996; Lichtman and Colman, 2000; Sanes and Lichtman, 1999; Yu et al., 2004). However, while activity-dependent changes in synaptic connectivity have been shown to occur in cultured hippocampal neurons (Burrone et al., 2002), activity-dependent refinement of memory circuits *in vivo* has not been examined. Here, we have established a mouse genetic system, where restricted populations of neurons in the hippocampal circuit can be inactivated. Using this system, we have examined the role of neural activity in the formation of appropriate hippocampal connections *in vivo*. We have shown that inactive EC and DG axons still reached their correct target, but that they were soon eliminated by activity-dependent competition with active axons. These results demonstrate for the first time that functional memory circuits in the mammalian brain are established as a result of activity-dependent competition between axons after their development.

Role of Action Potential-Dependent and Independent Activity

We have shown that TTX, which blocks action potentials (APs), efficiently inhibited the elimination of inactive axons. This indicates that APs play critical roles for synapse elimination, and strongly suggests that axons are refined by a spike activity-dependent competition. It would be interesting to identify the specific developmental windows over which TTX can prevent inactive axons from being retracted. Another fascinating question to address is a role for correlated firing between pre and postsynaptic neurons. It is possible that correlated firing contributes to refinement of hippocampal circuits, as it does in the visual system (Hata et al., 1999; Ruthazer et al., 2003). Future approaches to address this question include examining inactive (TeTxLC-expressing) axon elimination in our transgenic mice after suppressing postsynaptic neurons with GABA receptor agonists, glutamate receptor antagonists, or the inward rectifying potassium channel Kir2.1.

In addition, our results suggest that spike activity-independent mechanisms, such as miniature neurotransmission, might also be involved in activity-dependent refinement of hippocampal circuits. TeTxLC prevents the fusion of synaptic vesicles, and thus blocks both AP-dependent and independent synaptic release. Interestingly, TTX, which does not inhibit AP-independent synaptic release, did not appear to completely inhibit the elimination of TeTxLC-expressing axons in EC::TeTxLC-tau-lacZ and DG-A::TeTxLC-tau-lacZ mice.

Relative to P12 brains, the lacZ intensities at P16 were 124% in EC::tau-lacZ (no TeTxLC) mice and 95% in TTX-treated EC::TeTxLC-tau-lacZ mice (Figures 1G and 2C). Relative to P15 brains, the staining intensities at P23 were 94% in DG-A::tau-lacZ (no TeTxLC) mice and 70% in TTX-treated DG-A::TeTxLC-tau-lacZ mice (Figure S3C). Thus, AP-independent neurotransmitter release might also contribute to axon refinement. The neurotransmission that is important for activity-dependent refinement in neural circuits is typically assumed to be driven by presynaptic spiking. However, AP-independent neurotransmitter release (i.e., miniature neurotransmission) has been shown to play a role in activity-dependent input stabilization (Saitoe et al., 2001; McKinney et al., 1999; Sutton et al., 2006). It will be interesting to examine the role of miniature neurotransmission in synapse refinement in the hippocampus.

Neurogenesis and Activity-Dependent Refinement of DG Axons

While our results suggest that activity-dependent competition is a general principle of circuit refinement in the hippocampus, we also found a novel form of competition between DG axons in the refinement of the DG-CA3 projection. We conclude that activity-dependent competitions in DG-CA3 connections occur mostly between axons of mature and young DGCs because: (i) blocking neurogenesis with AraC or nestin-tk effectively inhibited the elimination of inactive axons in DG-S::TeTxLC-tau-lacZ mice, in which only 37% of mature DGCs express TeTxLC (Figures 8D–8G), (ii) the rate of inactive DG axon elimination was not affected by the percentage of mature axons that were inactivated (Figure 3H), and (iii) newborn DGCs rapidly form synapses in CA3 during refinement (P15 to P23; Figure 7).

The number of large boutons formed in CA3 by P23 by a DGC born at P15 was ~20 (Figures 7A and 7B), which is more than that of a mature DGC (11–15; Acsady et al., 1998). In addition, in DG-A::TeTxLC-tau-lacZ mice, in which many mossy fiber synapses are inactivated, neurogenesis was significantly enhanced during refinement: ~15% of total DGCs present at P23 were born between P15 and P22 (Figure 6H). Therefore, it appears that young DGCs promptly form sufficient synapses in CA3 to efficiently eliminate inactive synapses of mature DGCs during refinement. While our study focused on competition in CA3, it would be intriguing to examine whether competition takes place not only in CA3, but also in the hilus.

Taken together, our results demonstrate that, during development, young DG neurons compete with mature DG axons effectively. This may explain how newly generated young DG neurons are efficiently integrated into pre-existing circuitry in adults (Ge et al., 2006; Toni et al., 2008). Whether this form of competition and refinement occurs in the adult DG is an important next question to be answered.

Converging lines of evidence now suggest that DG neurogenesis is essential for several types of learning, memory formation and emotional processing (Doetsch and Hen, 2005; Kempermann et al., 2004; Lledo et al., 2006; Santarelli et al., 2003; Shors et al., 2001; Kitamura et al., 2009). In addition, adult-born DGCs during an immature stage of development are shown to play important roles in learning and memory (Deng et al., 2009). These results may imply that the activity-dependent competitive refinement of the DG-CA3 projection we have identified might contribute to cognitive functions requiring rapid and efficient circuit integration of newborn DGCs.

EXPERIMENTAL PROCEDURES

Animal Care

All animal care and use was in accordance with the institutional guidelines and approved by the University Committee on Use and Care of Animals.

tTA/tetO Transgenic Mice

tTA-EC (Yasuda and Mayford, 2006), tetO-nls-lacZ (Mayford et al., 1996), tetO-tau-lacZ (Yasuda and Mayford, 2006) and tetO-TeTxLC-tau-lacZ (Yu et al., 2004) lines were described previously.

tTA-DG lines were generated using a BAC clone 394B7 (Invitrogen) that includes the SIRPα gene. We used this clone because SIRPα proteins are highly expressed in the hippocampus (data not shown; Comu et al., 1997). The tTA gene was introduced upstream of the translation initiation site of the SIRPα gene by a homologous recombination in *E. coli* as described previously (Yasuda and Mayford, 2006). Generated transgenic lines were screened to identify lines that express tTA in the DG by mating them with the tetO-nls-lacZ transgenic line.

tTA and tetO lines were mated to generate bitransgenic mice. Bitransgenic mice were identified by genomic PCR and used for the experiments.

LacZ Staining

To visualize axons expressing tau-lacZ, 200 μm thick horizontal sections of the hippocampus were prepared with a tissue chopper (Stoelting). Sections were incubated with X-gal solution (5 mM potassium-ferricyanide, 5 mM potassium-ferrocyanide, 2 mM $MgCl_2$, 0.1% X-gal) for 2 hours at 37°C. After the incubation, tissues were fixed with 4% paraformaldehyde/phosphate-buffered saline (PBS) for 16 hours. For nls-lacZ staining, mouse brains were rapidly frozen in OCT embedding compound (Richard-Allan Scientific). 20 μm horizontal sections were cut on a cryostat and mounted onto microscope slides, fixed in 2% paraformaldehyde/PBS for 2 min on ice. Fixed sections were washed twice with PBS and incubated with X-gal solution for 3–5 hours at 37°C. X-gal stained slides were counterstained with Nuclear Fast Red.

Immunohistochemistry

Immunohistochemistry was performed as described (Umemori et al., 2004; Terauchi et al., 2010). Mice were euthanized and perfused transcardially with PBS followed by 4% paraformaldehyde/PBS. Brains were removed and post-fixed with 4% paraformaldehyde/PBS for 16 hours. After cryoprotection in 30% sucrose, brains were frozen in OCT embedding compound. 16 μm horizontal sections were cut on a cryostat and stored at −80°C until use. Sections were blocked in 2% BSA, 2% goat serum and 0.1% Triton X-100 in PBS for 1 hour, followed by the incubation with primary antibodies at 4°C for 16 hours in the same solution. Sections were washed in PBS and secondary antibodies were applied in PBS for 1 hour. Nuclei were stained with DAPI. Antibodies and dilutions used are: β-gal (Sigma, 1:500), NeuN (Chemicon, 1:1000), calretinin (Millipore, 1:500), doublecortin (Santa Cruz, 1:200), Ki67 (Thermo scientific, 1:200), VGLUT1 (Millipore, 1:4500), and bassoon (Assay Designs, 1:500). Stained sections were observed with an epifluorescence or confocal microscope (Olympus).

Electrophysiological Recording

Hippocampi were isolated from P11–12 (EC lines) or P15–17 (DG lines) mice, and 400 μm transverse slices were cut using a tissue chopper. Slices were then allowed to recover in an interface chamber for a minimum of two hours at 25°C. For field recordings, slices were placed in a chamber and perfused constantly with oxygenated artificial cerebral spinal fluid (aCSF) heated to 27–28°C. aCSF contained (in mM) 119 NaCl, 2.5 KCl, 1 Na_2PO_4, 26.3 $NaHCO_3$, 11 glucose, 1.3 $MgSO_4$, and 2.5 $CaCl_2$. To obtain input-output curves, fEPSPs were stimulated using a cluster electrode (FHC). For the EC line recording, both the stimulating electrode and the recording electrode (containing 3 M NaCl) were placed in the molecular layer of the DG. For the DG line experiments, the stimulating electrode was placed in the hilus of the DG and the recording electrode was placed in the stratum radiatum of CA3. Responses were collected with a MultiClamp 700B amplifier (Axon Instruments), and analyzed using Clampfit software (Axon Instruments). Statistical significance was determined using a two-way ANOVA.

5-Bromo-2-deoxyuridine Labeling and Immunohistochemistry

To examine DG cell survival (Figures 4E and 4F), WT and DG-A::TeTxLC-tau-lacZ mice (15 mice each) received a single injection of 5-bromo-2-deoxyuridine (BrdU) (300 mg/kg) at P7–8. Mice were perfused with 4% paraformaldehyde/PBS at P15, P20 and P25 (5 mice for each day per each genotype). Their brains were post-fixed with 4% paraformaldehyde/PBS for 16 hours, cryoprotected in 30% sucrose, and frozen in the OCT embedding compound. 50 μm horizontal sections were cut with a cryostat and placed in PBS (floating). Every sixth section was incubated with 2 M HCl for 30 min at 37 °C, washed in 0.1 M Tris buffer pH 8.0 for 10 min and washed three times in PBS for 3 min. Sections were then blocked in 2% BSA, 2% goat serum and 0.1% Triton X-100 in PBS for 1 hour, and incubated with the anti-BrdU (rat monoclonal; 1:400 Chemicon) and NeuN antibody at 4°C for 16 hours. After washing in PBS, sections were incubated with the goat anti-rat Alexa Fluor 488 and goat anti-mouse IgG_1 Alexa Fluor 568 secondary antibodies for 1 hour. Sections were washed again in PBS and mounted on slides with Prolong antifade reagent (Invitrogen). BrdU-labeled cells in the granule cell layer of the DG were manually counted under a fluorescence microscope with a 40× objective lens.

To examine the degree of neurogenesis (Figure 6H), BrdU (100 mg/kg) was injected into DG-A::TeTxLC-tau-lacZ and WT litters from P15 to P22 (8 days total of injection). Horizontal brain sections from P23 animals were stained with the anti-BrdU antibody as descried above.

DiI Labeling and Immunohistochemistry

Mice were euthanized and perfused with 4% paraformaldehyde/PBS. Their brains were dissected out and post-fixed with 4% PFA/PBS for 1 hour at 4°C. 100 μm thick horizontal sections were cut on a vibratome and stored in PBS. Sections were placed in a drop of PBS on a 10 mm Petri dish and chloromethylbenzamido-DiI (CM-DiI; Invitrogen) coated Elvax (0.1 × 0.1 × 0.1 mm) was placed onto the hilar region of the sections and left for 2 hours at 25°C or for 16 hours at 4°C. After CM-DiI coated Elvax was removed from the sections, the sections were fixed again with 4% paraformaldehyde/PBS for 1 hour, blocked in 2% BSA, 2% goat serum and 0.1% Triton X-100 in PBS for 1 hour, and incubated with the anti-β-gal antibody at 4°C for 16 hours. Anti-mouse IgG_1 Alexa Fluor 488 was used as the secondary antibody. Stained sections were mounted on a slide with Prolong antifade reagent. Images were taken with an Olympus confocal microscope using a 40× lens.

Image Quantification

For quantification of lacZ staining, color images taken by a digital camera (E990 Nikon) with a dissecting microscope (Olympus) were converted to gray scale images and then inverted with ImageJ software (NIH). The average signal intensity in the stratum lucidum layer of CA3 was calculated with ImageJ. The average signal intensity in the stratum radiatum of CA3 in the same section was calculated and subtracted as the background.

For quantification of β-gal immunostaining with DG lines (Figures 5, 6, and 8), images were acquired on a BX61 microscope (Olympus) with a 20× objective lens using the same exposure time for each experiment. The intensity of staining in the hilar region of the hippocampus was analyzed with ImageJ software. The intensity in the neighboring area without stained axons (in the stratum radiatum of CA3) in the same section was calculated and subtracted as the background (see Figure S3B).

Drug Treatments

Mice were anesthetized with ketamine/xylazine (60 mg/kg ketamine, 10 mg/kg xylazine), placed in a hand-made frame and their skull was exposed. A hole was generated with a 26-gage needle (−1.2 mm from bregma, 1.0 mm lateral from the midline, and 1.5 mm ventral from the skull surface for EC::TeTxLC-tau-lacZ mice; −2 mm from bregma, 1.5 mm lateral from the midline, and 2 mm ventral from the skull surface for DG::TeTxLC-tau-lacZ mice) onto the left hemisphere. Optimal locations were determined by preliminary experiments with Trypan Blue injections. TTX (0.5 μl of 5 μM TTX in PBS) was injected every 24 hours from P9 to P12, P14, or P16 (4, 6, or 8 days total of injection) with a Hamilton syringe (75RN, 7762-03) mounted on a micromanipulator.

To suppress neurogenesis, AraC was injected either icv or ip (icv, 1 μl of 10 μg/μl AraC in PBS; ip, 40 mg/kg body weight AraC in PBS; similar results were obtained by either method) everyday from P15 to P22 (8 days total). Icv injections were performed as described above. For ip injections, AraC was injected every 12 hours. TMZ was injected ip everyday (25 mg/kg) from P15 to P22 (8 days total). Mice were sacrificed at P23 and analyzed.

Preparation of TTX-Elvax

TTX-Elvax was prepared as described (Echegoyen et al., 2007). 50 mg of Elvax 40W (DuPont) was dissolved in 500 μl of methylene chloride, then 1 mg TTX (Tocris) was added. Evenly suspended mixture solution was plated onto a slide glass and stored at −20°C. TTX-Elvax was sectioned to 500 × 500 μm blocks and washed in PBS at room temperature a day before implantation.

TTX-Elvax Implantation

P15 Mice were anesthetized with ketamine/xylazine, placed in a hand-made frame, and the skull was exposed. Three sides of a square, which is located from −1.5 mm to −3.5 mm from the bregma and from 1 mm to 3 mm lateral from the midline on the skull, were cut (see Figure S3A) and the skull flap is flipped. A 26-gage needle, which was bent 1.5 mm from the tip to a 90° angle, was used to cut the same three sides on the exposed cortex. The resultant cortical slab was lifted and TTX-Elvax or control Elvax was placed on the hippocampus under the lifted cortical slab. The wound was closed, the animals were placed on a heated pad for recovery and returned to their cage.

Retrovirus Labeling of Newborn DGC Progenitors

P15 mice were anesthetized with ketamine/xylazine and 1 μl of GFP-expressing retrovirus (Kron et al., 2010) was injected into both dentate gyri (1.6 mm posterior to the bregma, 1.1 mm lateral from the midline, and 2.3 mm ventral from the skull surface). The mice were perfused with 4% paraformaldehyde/PBS at P23, and their brains were processed for immunostaining (50 μm horizontal sections). Images were taken with an Olympus confocal microscope using a 40× lens.

Nestin-tk Transgenic Mice and Ganciclovir Treatment

Nestin-tk transgenic mice were described previously (Singer et al., 2009). DG-S::TeTxLC-tau-lacZ double transgenic mice were mated with nestin-tk mice to obtain triple transgenic mice (DG-S::TeTxLC-tau-lacZ::nestin-tk). DG-S::TeTxLC-tau-lacZ and DG-S::TeTxLC-tau-lacZ::nestin-tk mice were injected with 80 mg/kg ganciclovir intraperitoneally once daily from P15 to P22. Horizontal brain sections from P23 mice were processed for immunostaining.

Supplementary Material

Refer to Web version on PubMed Central for supplementary material.

Acknowledgments

We thank M. Nakafuku and J. R. Sanes for critical comments on the manuscript; M. Mayford for tTA-EC, tetO-nls-lacZ and tetO-tau-lacZ lines; J. Gogos for the tetO-TeTxLC-tau-lacZ line; M. Zhang and C. Kanki for technical assistance; W. Filipiak, G. Gavrilina, M. Van Keuren and the Transgenic Animal Model Core of the University of Michigan for preparation of transgenic mice. Core support was provided by the University of Michigan Center for Organogenesis. This work was supported by the Ester A. & Joseph Klingenstein Fund, the Edward Mallinckrodt Jr. Foundation, the March of Dimes Foundation, the Whitehall Foundation, and NIH grants MH091429 and NS070005 (H.U.).

References

Acsady L, Kamondi A, Sik A, Freund T, Buzsaki G. GABAergic cells are the major postsynaptic targets of mossy fibers in the rat hippocampus. J Neurosci. 1998; 18:3386–3403. [PubMed: 9547246]

Amaral DG, Dent JA. Development of the mossy fibers of the dentate gyrus: I. A light and electron microscopic study of the mossy fibers and their expansions. J Comp Neurol. 1981; 195:51–86. [PubMed: 7204652]

Amaral DG, Witter MP. The three-dimensional organization of the hippocampal formation: a review of anatomical data. Neuroscience. 1989; 31:571–591. [PubMed: 2687721]

Bishop DL, Misgeld T, Walsh MK, Gan WB, Lichtman JW. Axon branch removal at developing synapses by axosome shedding. Neuron. 2004; 44:651–661. [PubMed: 15541313]

Braak H, Braak E. Neuropathological stageing of Alzheimer-related changes. Acta Neuropathol (Berl). 1991; 82:239–259. [PubMed: 1759558]

Brandt MD, Jessberger S, Steiner B, Kronenberg G, Reuter K, Bick-Sander A, von der Behrens W, Kempermann G. Transient calretinin expression defines early postmitotic step of neuronal differentiation in adult hippocampal neurogenesis of mice. Mol Cell Neurosci. 2003; 24:603–613. [PubMed: 14664811]

Brun VH, Otnass MK, Molden S, Steffenach HA, Witter MP, Moser MB, Moser EI. Place cells and place recognition maintained by direct entorhinal-hippocampal circuitry. Science. 2002; 296:2243–2246. [PubMed: 12077421]

Buffelli M, Burgess RW, Feng G, Lobe CG, Lichtman JW, Sanes JR. Genetic evidence that relative synaptic efficacy biases the outcome of synaptic competition. Nature. 2003; 424:430–434. [PubMed: 12879071]

Burrone J, O'Byrne M, Murthy VN. Multiple forms of synaptic plasticity triggered by selective suppression of activity in individual neurons. Nature. 2002; 420:414–418. [PubMed: 12459783]

Comu S, Weng W, Olinsky S, Ishwad P, Mi Z, Hempel J, Watkins S, Lagenaur CF, Narayanan V. The murine P84 neural adhesion molecule is SHPS-1, a member of the phosphatase-binding protein family. J Neurosci. 1997; 17:8702–8710. [PubMed: 9348339]

Deng W, Saxe MD, Gallina IS, Gage FH. Adult-born hippocampal dentate granule cells undergoing maturation modulate learning and memory in the brain. J Neurosci. 2009; 29:13532–13542. [PubMed: 19864566]

deToledo-Morrell L, Stoub TR, Bulgakova M, Wilson RS, Bennett DA, Leurgans S, Wuu J, Turner DA. MRI-derived entorhinal volume is a good predictor of conversion from MCI to AD. Neurobiol Aging. 2004; 25:1197–1203. [PubMed: 15312965]

Doetsch F, Hen R. Young and excitable: the function of new neurons in the adult mammalian brain. Curr Opin Neurobiol. 2005; 15:121–128. [PubMed: 15721754]

Echegoyen J, Neu A, Graber KD, Soltesz I. Homeostatic plasticity studied using *in vivo* hippocampal activity-blockade: synaptic scaling, intrinsic plasticity and age-dependence. PLoS One. 2007; 2:e700. [PubMed: 17684547]

Eichenbaum H. A cortical-hippocampal system for declarative memory. Nat Rev Neurosci. 2000; 1:41–50. [PubMed: 11252767]

Elmer GI, Sydnor J, Guard H, Hercher E, Vogel MW. Altered prepulse inhibition in rats treated prenatally with the antimitotic Ara-C: an animal model for sensorimotor gating deficits in schizophrenia. Psychopharmacology (Berl). 2004; 174:177–189. [PubMed: 14985933]

Fyhn M, Molden S, Witter MP, Moser EI, Moser MB. Spatial representation in the entorhinal cortex. Science. 2004; 305:1258–1264. [PubMed: 15333832]

Gage FH. Mammalian neural stem cells. Science. 2000; 287:1433–1438. [PubMed: 10688783]

Garthe A, Behr J, Kempermann G. Adult-generated hippocampal neurons allow the flexible use of spatially precise learning strategies. PLoS One. 2009; 4:e5464. [PubMed: 19421325]

Ge S, Goh EL, Sailor KA, Kitabatake Y, Ming GL, Song H. GABA regulates synaptic integration of newly generated neurons in the adult brain. Nature. 2006; 439:589–593. [PubMed: 16341203]

Gomez-Isla T, Price JL, McKeel DW Jr, Morris JC, Growdon JH, Hyman BT. Profound loss of layer II entorhinal cortex neurons occurs in very mild Alzheimer's disease. J Neurosci. 1996; 16:4491–4500. [PubMed: 8699259]

Hafting T, Fyhn M, Molden S, Moser MB, Moser EI. Microstructure of a spatial map in the entorhinal cortex. Nature. 2005; 436:801–806. [PubMed: 15965463]

Hastings NB, Gould E. Rapid extension of axons into the CA3 region by adult-generated granule cells. J Comp Neurol. 1999; 413:146–154. [PubMed: 10464376]

Hashimoto K, Kano M. Postnatal development and synapse elimination of climbing fiber to Purkinje cell projection in the cerebellum. Neurosci Res. 2005; 53:221–228. [PubMed: 16139911]

Hata Y, Tsumoto T, Stryker MP. Selective pruning of more active afferents when cat visual cortex is pharmacologically inhibited. Neuron. 1999; 22:375–381. [PubMed: 10069342]

Hua JY, Smear MC, Baier H, Smith SJ. Regulation of axon growth *in vivo* by activity-based competition. Nature. 2005; 434:1022–1026. [PubMed: 15846347]

Jansen JK, Fladby T. The perinatal reorganization of the innervation of skeletal muscle in mammals. Prog Neurobiol. 1990; 34:39–90. [PubMed: 2406795]

Kantor DB, Kolodkin AL. Curbing the excesses of youth: molecular insights into axonal pruning. Neuron. 2003; 38:849–852. [PubMed: 12818170]

Katz LC, Shatz CJ. Synaptic activity and the construction of cortical circuits. Science. 1996; 274:1133–1138. [PubMed: 8895456]

Kee N, Sivalingam S, Boonstra R, Wojtowicz JM. The utility of Ki-67 and BrdU as proliferative markers of adult neurogenesis. J Neurosci Methods. 2002; 115:97–105. [PubMed: 11897369]

Kempermann G, Gast D, Kronenberg G, Yamaguchi M, Gage FH. Early determination and long-term persistence of adult-generated new neurons in the hippocampus of mice. Development. 2003; 130:391–399. [PubMed: 12466205]

Kempermann G, Wiskott L, Gage FH. Functional significance of adult neurogenesis. Curr Opin Neurobiol. 2004; 14:186–191. [PubMed: 15082323]

Kitamura T, Saitoh Y, Takashima N, Murayama A, Niibori Y, Ageta H, Sekiguchi M, Sugiyama H, Inokuchi K. Adult neurogenesis modulates the hippocampus-dependent period of associative fear memory. Cell. 2009; 139:814–827. [PubMed: 19914173]

Kokoeva MV, Yin H, Flier JS. Neurogenesis in the hypothalamus of adult mice: potential role in energy balance. Science. 2005; 310:679–683. [PubMed: 16254185]

Kron MM, Zhang H, Parent JM. The developmental stage of dentate granule cells dictates their contribution to seizure-induced plasticity. J Neurosci. 2010; 30:2051–2059. [PubMed: 20147533]

Li Y, Mu Y, Gage FH. Development of neural circuits in the adult hippocampus. Curr Top Dev Biol. 2009; 87:149–174. [PubMed: 19427519]

Lichtman JW, Colman H. Synapse elimination and indelible memory. Neuron. 2000; 25:269–278. [PubMed: 10719884]

Lie DC, Song H, Colamarino SA, Ming GL, Gage FH. Neurogenesis in the adult brain: new strategies for central nervous system diseases. Annu Rev Pharmacol Toxicol. 2004; 44:399–421. [PubMed: 14744252]

Lledo PM, Alonso M, Grubb MS. Adult neurogenesis and functional plasticity in neuronal circuits. Nat Rev Neurosci. 2006; 7:179–193. [PubMed: 16495940]

Lohof AM, Delhaye-Bouchaud N, Mariani J. Synapse elimination in the central nervous system: functional significance and cellular mechanisms. Rev Neurosci. 1996; 7:85–101. [PubMed: 8819204]

Lorenzetto E, Caselli L, Feng G, Yuan W, Nerbonne JM, Sanes JR, Buffelli M. Genetic perturbation of postsynaptic activity regulates synapse elimination in developing cerebellum. Proc Natl Acad Sci U S A. 2009; 106:16475–16480. [PubMed: 19805323]

Mayford M, Bach ME, Huang YY, Wang L, Hawkins RD, Kandel ER. Control of memory formation through regulated expression of a CaMKII transgene. Science. 1996; 274:1678–1683. [PubMed: 8939850]

McHugh TJ, Jones MW, Quinn JJ, Balthasar N, Coppari R, Elmquist JK, Lowell BB, Fanselow MS, Wilson MA, Tonegawa S. Dentate gyrus NMDA receptors mediate rapid pattern separation in the hippocampal network. Science. 2007; 317:94–99. [PubMed: 17556551]

McKinney RA, Capogna M, Dürr R, Gähwiler BH, Thompson SM. Miniature synaptic events maintain dendritic spines via AMPA receptor activation. Nat Neurosci. 1999; 2:44–49. [PubMed: 10195179]

Ming GL, Song H. Adult neurogenesis in the mammalian central nervous system. Annu Rev Neurosci. 2005; 28:223–250. [PubMed: 16022595]

Nakashiba T, Young JZ, McHugh TJ, Buhl DL, Tonegawa S. Transgenic inhibition of synaptic transmission reveals role of CA3 output in hippocampal learning. Science. 2008; 319:1260–1264. [PubMed: 18218862]

Nakazawa K, Quirk MC, Chitwood RA, Watanabe M, Yeckel MF, Sun LD, Kato A, Carr CA, Johnston D, Wilson MA, Tonegawa S. Requirement for hippocampal CA3 NMDA receptors in associative memory recall. Science. 2002; 297:211–218. [PubMed: 12040087]

O'Keefe, J.; Nadel, L. The Hippocampus as a Cognitive Map. Oxford, UK: Oxford University Press; 1978.

Purves D, Lichtman JW. Elimination of synapses in the developing nervous system. Science. 1980; 210:153–157. [PubMed: 7414326]

Ruthazer ES, Akerman CJ, Cline HT. Control of axon branch dynamics by correlated activity in vivo. Science. 2003; 301:66–70. [PubMed: 12843386]

Saitoe M, Schwarz TL, Umbach JA, Gundersen CB, Kidokoro Y. Absence of junctional glutamate receptor clusters in Drosophila mutants lacking spontaneous transmitter release. Science. 2001; 293:514–517. [PubMed: 11463917]

Sanes JR, Lichtman JW. Development of the vertebrate neuromuscular junction. Annu Rev Neurosci. 1999; 22:389–442. [PubMed: 10202544]

Santarelli L, Saxe M, Gross C, Surget A, Battaglia F, Dulawa S, Weisstaub N, Lee J, Duman R, Arancio O, et al. Requirement of hippocampal neurogenesis for the behavioral effects of antidepressants. Science. 2003; 301:805–809. [PubMed: 12907793]

Schiavo G, Benfenati F, Poulain B, Rossetto O, Polverino de Laureto P, DasGupta BR, Montecucco C. Tetanus and botulinum-B neurotoxins block neurotransmitter release by proteolytic cleavage of synaptobrevin. Nature. 1992; 359:832–835. [PubMed: 1331807]

Shors TJ, Miesegaes G, Beylin A, Zhao M, Rydel T, Gould E. Neurogenesis in the adult is involved in the formation of trace memories. Nature. 2001; 410:372–376. [PubMed: 11268214]

Singer BH, Jutkiewicz EM, Fuller CL, Lichtenwalner RJ, Zhang H, Velander AJ, Li X, Gnegy ME, Burant CF, Parent JM. Conditional ablation and recovery of forebrain neurogenesis in the mouse. J Comp Neurol. 2009; 514:567–582. [PubMed: 19363795]

Squire LR, Stark CE, Clark RE. The medial temporal lobe. Annu Rev Neurosci. 2004; 27:279–306. [PubMed: 15217334]

Sutton MA, Ito HT, Cressy P, Kempf C, Woo JC, Schuman EM. Miniature neurotransmission stabilizes synaptic function via tonic suppression of local dendritic protein synthesis. Cell. 2006; 125:785–799. [PubMed: 16713568]

Sweeney ST, Broadie K, Keane J, Niemann H, O'Kane CJ. Targeted expression of tetanus toxin light chain in Drosophila specifically eliminates synaptic transmission and causes behavioral defects. Neuron. 1995; 14:341–351. [PubMed: 7857643]

Terauchi A, Johnson-Venkatesh EM, Toth AB, Javed D, Sutton MA, Umemori H. Distinct FGFs promote differentiation of excitatory and inhibitory synapses. Nature. 2010; 465:783–787. [PubMed: 20505669]

Toni N, Laplagne DA, Zhao C, Lombardi G, Ribak CE, Gage FH, Schinder AF. Neurons born in the adult dentate gyrus form functional synapses with target cells. Nat Neurosci. 2008; 11:901–907. [PubMed: 18622400]

Umemori H, Linhoff MW, Ornitz DM, Sanes JR. FGF22 and its close relatives are presynaptic organizing molecules in the mammalian brain. Cell. 2004; 118:257–270. [PubMed: 15260994]

van Groen T, Miettinen P, Kadish I. The entorhinal cortex of the mouse: organization of the projection to the hippocampal formation. Hippocampus. 2003; 13:133–149. [PubMed: 12625464]

Witter MP, Groenewegen HJ, Lopes da Silva FH, Lohman AH. Functional organization of the extrinsic and intrinsic circuitry of the parahippocampal region. Prog Neurobiol. 1989; 33:161–253. [PubMed: 2682783]

Yasuda M, Mayford MR. CaMKII activation in the entorhinal cortex disrupts previously encoded spatial memory. Neuron. 2006; 50:309–318. [PubMed: 16630840]

Yu CR, Power J, Barnea G, O'Donnell S, Brown HE, Osborne J, Axel R, Gogos JA. Spontaneous neural activity is required for the establishment and maintenance of the olfactory sensory map. Neuron. 2004; 42:553–566. [PubMed: 15157418]

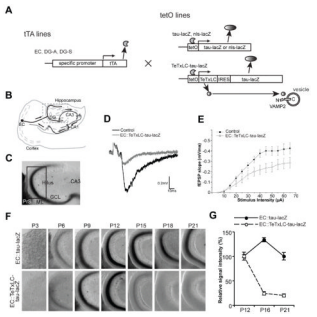

Figure 1. Elimination of Inactive EC axons *In Vivo*, as Shown by Using a Mouse Genetic System

(A) Schematic of the tTA/tetO transgenic system. tTA lines (EC, DG-A and DG-S lines), which have specific expression patterns of tetracycline-controlled transactivator (tTA) in the entorhinal cortex (EC) or dentate gyrus (DG), are mated with tetO lines (nls-lacZ, tau-lacZ and TeTxLC-tau-lacZ lines), which express transgenes under the tTA-activated tetO promoter. Tetanus toxin light chain (TeTxLC) cleaves VAMP2 to inhibit synaptic release. Tau-lacZ labels axons, and nls (nuclear localization signal)-lacZ labels nuclei.

(B) Illustration of the memory circuit. The memory circuit consists of unidirectional synaptic connections: from the EC to the DG to CA3 to CA1 to the EC.

(C to G) The tTA-EC mouse, in which tTA is expressed by about 43% of the superficial layer neurons of the medial EC, was mated with the tetO-tau-lacZ or tetO-TeTxLC-tau-lacZ mouse.

(C) A typical picture of a lacZ-stained DG section (horizontal) from an EC::tau-lacZ mouse at P9. The pictured area corresponds to the boxed area in (B). LacZ-expressing medial EC axons run through the presubiculum (PrS) and project to the middle third of the molecular layer (ML) of the DG (black signals). GCL, granule cell layer. Pictured areas in (F) and Figure 2B correspond to the boxed area in (C).

(D and E) Evoked fEPSPs were recorded in acute slices from the molecular layer of the DG of EC::TeTxLC-tau-lacZ and control littermates (P11–P12). (D) Sample traces of fEPSP recordings. (E) Input-output curves. Input-output relationships were measured by varying the stimulus input intensity and measuring the fEPSP slope. 26 slices from EC::TeTxLC-tau-lacZ and 25 slices from control littermates. Each was from 5 mice. The fEPSP slope was decreased in the EC::TeTxLC-tau-lacZ mice relative to control littermates by ~35%. $p < 0.001$ by two way ANOVA.

(F) Elimination of TeTxLC-expressing EC axons from the DG after they develop. In both EC::tau-lacZ and EC::TeTxLC-tau-lacZ mice, EC axons reached the DG by P9. Active EC axons (in EC::tau-lacZ mice) increased and remained in the DG from P12 to P21. However, inactive EC axons (in EC::TeTxLC-tau-lacZ mice) were eliminated between P12 and P18.

(G) Quantification of the amount of lacZ-expressing EC axons in the ML of the DG in EC::tau-lacZ and EC::TeTxLC-tau-lacZ mice at P12, P16 and P21. Intensities were normalized against the intensity of corresponding P12 mice. Data are mean ± SEM. The numbers of mice used for analysis were: EC::tau-lacZ, P12, 12 mice; P16, 5 mice; P21, 9 mice; EC::TeTxLC-tau-lacZ, P12, 7 mice; P16, 6 mice; P21, 8 mice.

See also Figure S1.

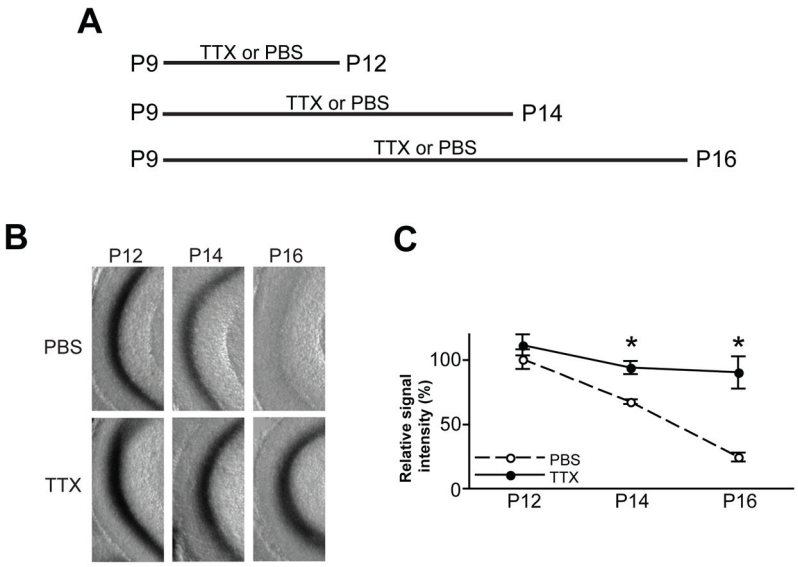

Figure 2. Global Suppression of Neural Activity Inhibits the Elimination of Inactive EC Axons

(A) Schematic time-line of the experiment. EC::TeTxLC-tau-lacZ mice were injected icv with PBS or tetrodotoxin (TTX) every 24 hours from P9 and their DGs were lacZ-stained at P12, P14, or P16 (4, 6, or 8 days total of PBS/TTX injections).

(B) PBS-injected mice showed the elimination of TeTxLC-expressing axons between P12 and P16. In contrast, TTX-injected mice maintained TeTxLC-expressing axons.

(C) Quantification of the lacZ staining intensity in the DG from results such as those shown in (B). Intensities were normalized against the intensity of P12 PBS-injected mice. Data are mean ± SEM. The numbers of mice analyzed were: PBS, P12, 7 mice; P14, 6 mice; P16, 6 mice; TTX, P12, 8 mice; P14, 7 mice; P16, 7 mice. Differs from the age-matched PBS-injected mice at *$p < 0.01$ by Student's t-test.

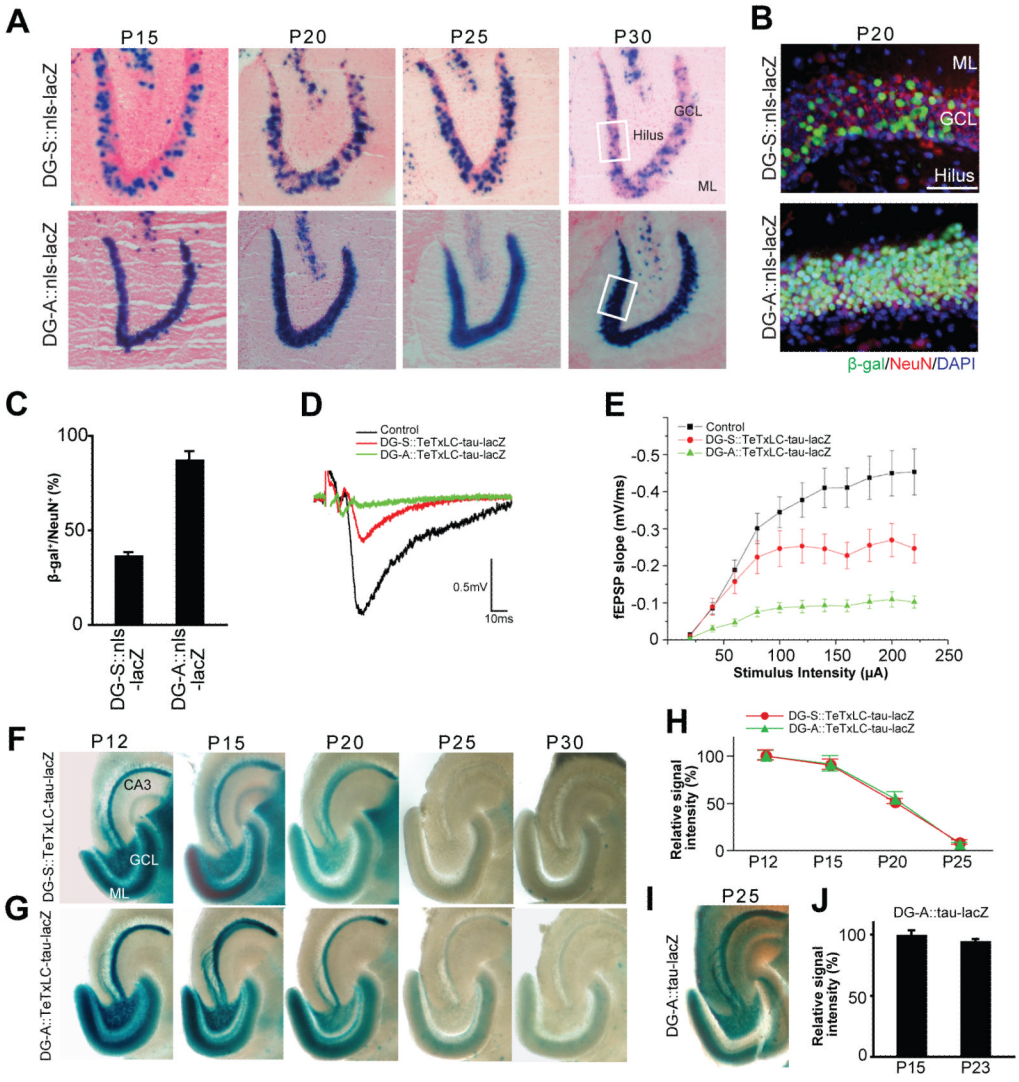

Figure 3. Activity-Dependent Elimination of Inactive DG Axons in Two tTA Lines that Express tTA in Different Numbers of DG Neurons

(A) Developmental expression patterns of tTA in the DG of two tTA lines, DG-S and DG-A. Expression patterns were examined by mating the DG-S and DG-A mouse with the nls-lacZ mouse. LacZ-stained horizontal sections between P15 and P30 are shown. Nuclei of tTA-expressing cells are stained in blue. In DG-S::nls-lacZ mice less than half of dentate neurons in the granule cell layer (GCL) express tTA, while in DG-A::nls-lacZ mice almost all dentate neurons do. Between P15 and P30, the percentage of tTA-expressing cells in the GCL was not changed in either transgenic mouse. ML, molecular layer.

(B) Immunostaining of DG sections from DG-S::nls-lacZ and DG-A::nls-lacZ mice for β-gal (green) and NeuN (red); nuclear DAPI staining is shown in blue. Pictured areas correspond to the boxed areas in (A). β-gal positive cells in the DG of both bitransgenic mice are NeuN positive, indicating that they are mature neurons. Scale bar is 50 μm.

(C) Percentage of β-gal positive neurons in the DG of DG-S::nls-lacZ and DG-A::nls-lacZ mice. Bars are mean ± SEM. Data are from 8 (DG-S) and 4 (DG-A) mice.

(D and E) Evoked fEPSPs were recorded in acute slices from CA3 of DG-A::TeTxLC-tau-lacZ, DG-S::TeTxLC-tau-lacZ, and control mice (P15–P17). (D) Sample traces of fEPSP recordings. (E) Input-output curves. Input-output relationships were measured by varying

the stimulus input intensity and measuring the fEPSP slope. 32 slices from DG-A::TeTxLC-tau-lacZ, 22 slices from DG-S::TeTxLC-tau-lacZ, and 52 slices from control mice. Each was from at least 5 mice. Relative to control mice, the fEPSP slope was decreased by ~80% and ~44% in the DG-A::TeTxLC-tau-lacZ and DG-S::TeTxLC-tau-lacZ mice, respectively.
(F and G) Developmental elimination of inactive DG axons. DG-S (F) and DG-A (G) mice were mated with TeTxLC-tau-lacZ mice to inactivate tTA-expressing neurons. Horizontal sections of the hippocampus from P12 to P30 were lacZ-stained. In both bitransgenic mice, inactive axons from the DG neurons still projected to CA3 by P12 (F and G). In DG-S::TeTxLC-tau-lacZ mice, in which a moderate number of DG neurons express TeTxLC, inactive axons were eliminated by P25 (F). In DG-A::TeTxLC-tau-lacZ mice, in which almost all DG neurons are inactivated, inactive axons were also eliminated by P25 (G).
(H) Quantification of the lacZ-staining intensity in the stratum lucidum layer of CA3 from P12 to P25. Data are shown as percentage of corresponding P12 mice. Data are mean ± SEM. The numbers of mice analyzed were: DG-A::TeTxLC-tau-lacZ, P12, 6 mice; P15, 5 mice; P20, 5 mice; P25, 5 mice; DG-S::TeTxLC-tau-lacZ, P12, 5 mice; P15, 5 mice; P20, 5 mice; P25, 5 mice.
(I and J) Maintenance of lacZ-expressing DG axons in DG-A::tau-lacZ (no TeTxLC) mice during development. (I) A horizontal section of the hippocampus from P25 DG-A::tau-lacZ mice was lacZ -stained. Active axons from DG neurons remained in CA3 at P25. (J) Horizontal sections from P15 and P23 DG-A::tau-lacZ mice were immunostained with the anti-β-gal antibody, and the staining intensity in the hilus was quantified. Intensities are normalized against the intensity of P15 mice. Bars are mean ± SEM. Data are from 5 mice.

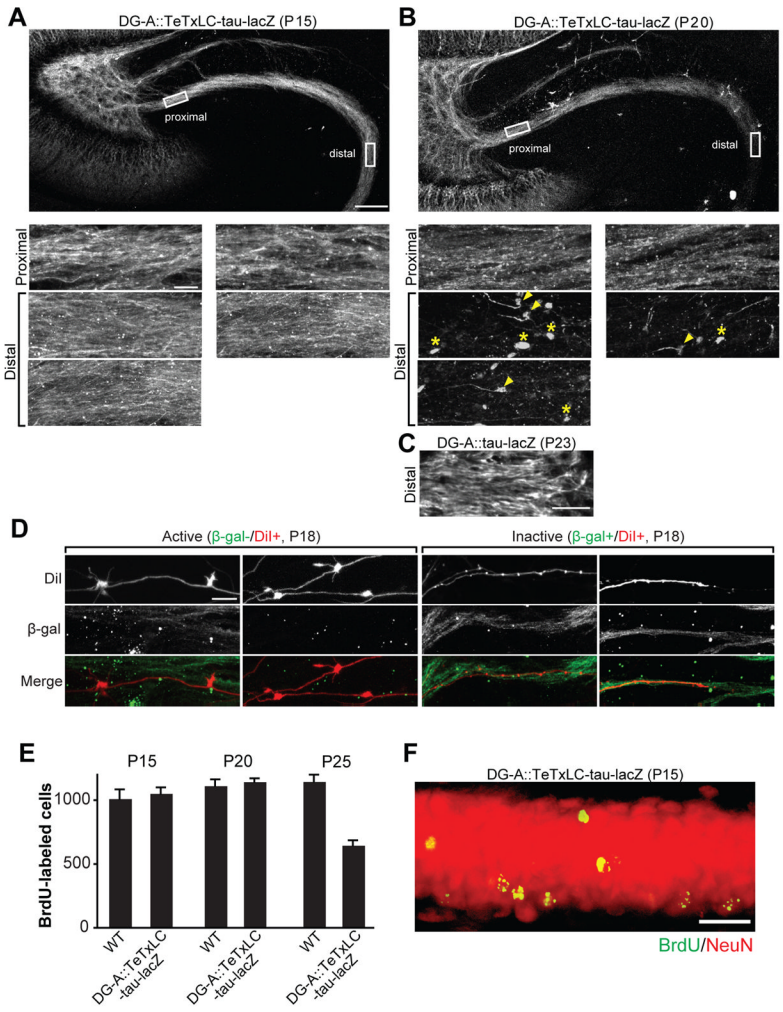

Figure 4. Elimination of Inactive DG Axons Is by Axon Retraction and Not Caused by DG Cell Death

(A and B) Representative confocal images of TeTxLC-expressing DG axons in the DG-A::TeTxLC-tau-lacZ line at P15 (A) and P20 (B). 50 μm thick horizontal vibratome sections were stained with the anti-β-gal antibody to visualize TeTxLC-tau-lacZ-expressing axons. Higher magnification pictures of the proximal and distal regions of the axons are shown in the bottom panels. At P20 (B), at the distal region of DG axons, there were retraction bulbs (arrowheads) and remnants of axons (axosomes; asterisks), which are signs of axon retraction. Scale bars are 100 μm (top), 10 μm (bottom panels).

(C) Confocal image of the distal region of DG axons in the DG-A::tau-lacZ line (no TeTxLC) at P23 (anti-β-gal staining). Without TeTxLC, the distal region of DG axons remained intact at P23. Scale bar is 10 μm.

(D) Confocal images of DiI-labeled active and inactive DG axons in DG-A::TeTxLC-tau-lacZ mice. Hippocampal sections (100 μm thick) were prepared from P18 DG-A::TeTxLC-tau-lacZ mice and their DG axons were sparsely labeled with DiI. The sections were stained for β-gal to identify inactive axons. Active axons (β-gal-/DiI+) had many large mossy fiber buttons, whereas no large buttons were found in inactive axons (β-gal+/DiI+). Scale bar is 10μm.

(E and F) Wild type (WT) and DG-A::TeTxLC-tau-lacZ mice (15 mice each) received a single injection of BrdU (300 mg/kg) at P7–8 to label dividing DG cells. Hippocampal

sections were prepared at P15, P20 and P25 (5 mice per day for each genotype) and stained for BrdU to evaluate DG cell survival. (E) The number of BrdU-positive DG cells at P15, P20 and P25. Similar numbers of BrdU-labeled DG neurons were found in WT and DG-A::TeTxLC-tau-lacZ mice at P20 when inactive DG axons were being retracted (B), suggesting that inactive DG axon retraction was not caused by DG cell death. The number of BrdU-positive cells in DG-A::TeTxLC-tau-lacZ mice was significantly decreased at P25, suggesting that inactive DG neurons were eventually eliminated after axon retraction. Bars are mean ± SEM. (F) Double staining for BrdU and NeuN of a DG section from DG-A::TeTxLC-tau-lacZ mice (P15). All BrdU-labeled DG neurons were NeuN positive. Scale bar is 20μm.

See also Figure S2.

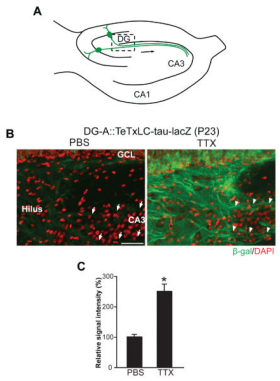

Figure 5. Global Suppression of Neural Activity Inhibits the Elimination of Inactive DG Axons in Mice in which Almost All DG Mature Neurons Are Inactivated

(A) Schematic illustration of the hippocampus indicating the pictured area in (B).

(B) PBS- or TTX-containing Elvax was implanted on the hippocampus of DG-A::TeTxLC-tau-lacZ mice at P15 and their hippocampi were stained with the anti-β-gal antibody (green) at P23 to visualize TeTxLC-expressing axons (8 days total of TTX-Elvax application). Nuclei were stained with DAPI (red). In PBS-treated mice, few TeTxLC-expressing axons remained in CA3 (arrows). In contrast, in TTX-treated mice, many TeTxLC-expressing axons were maintained in CA3 (arrowheads). Scale bar is 50 μm.

(C) Quantification of the intensity of β-gal staining in the hilar region of PBS- or TTX-treated DG-A::TeTxLC-tau-lacZ mice. Data are shown as percentage of PBS control. Bars are mean ± SEM. Data are from 6 mice. Differs from the PBS-treated mice at *$p < 0.01$ by Student's t-test.

See also Figure S3.

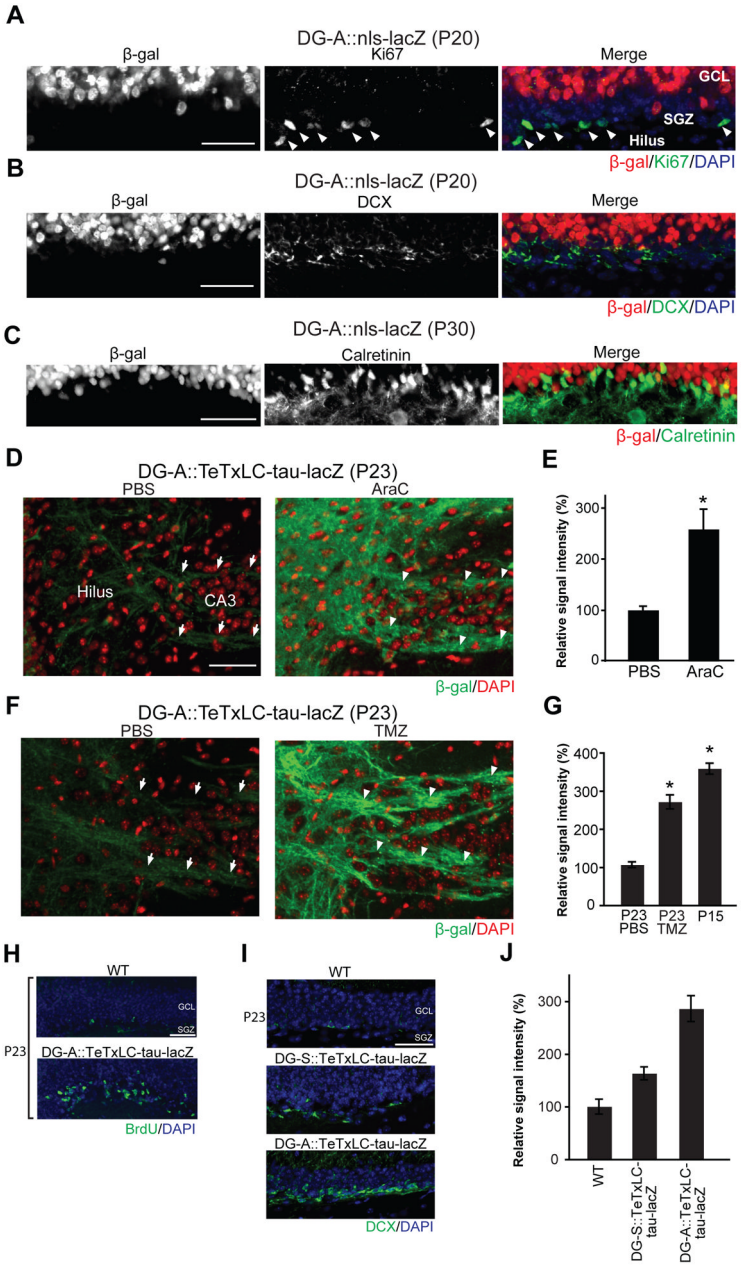

Figure 6. Suppression of Neurogenesis Inhibits the Elimination of Inactive DG Axons in Mice in which Almost All DG Mature Neurons Are Inactivated

(A) Double staining of the DG from P20 DG-A::nls-lacZ mice for β-gal (red) and a dividing cell marker Ki67 (green). The cell layer with Ki67-positive cells (subgranular zone, SGZ; arrowheads) did not contain β-gal positive cells.

(B and C) Double staining of the DG from DG-A::nls-lacZ mice for β-gal (red) and the young dentate granule cell markers, doublecortin (DCX; green; B) or calretinin (green; C). Most DCX and calretinin positive cells do not express β-gal.

(D to G) DG-A::TeTxLC-tau-lacZ mice were injected with PBS, AraC (D and E) or TMZ (F and G) from P15 to P22 (8 days total) and their DGs were stained with the anti-β-gal antibody (green) at P23. Nuclei were stained with DAPI (red). (D and F) PBS-injected mice eliminated β-gal positive inactive axons (arrows indicate few remaining axons), but AraC-

or TMZ-injected mice retained them (arrowheads). (E) Quantification of the β-gal immunostaining intensity in the hilar region of PBS- and AraC-treated DG-A::TeTxLC-tau-lacZ mice. Data are shown as percentage of PBS control. Bars are mean ± SEM. Data are from 5 mice. Differs from the PBS-injected mice at *$p < 0.01$ by Student's t-test. (G) Quantification of the β-gal immunostaining intensity in the hilar region of PBS- and TMZ-treated DG-A::TeTxLC-tau-lacZ mice (P23) and non-treated DG-A::TeTxLC-tau-lacZ mice (P15). Data are shown as percentage of P23 PBS control. Bars are mean ± SEM. The numbers of mice analyzed were: P23 PBS, 6 mice; P23 TMZ, 7 mice; P15, 5 mice. Differs from the PBS-injected mice at *$p < 0.01$ by ANOVA.
(H) Increased neurogenesis in DG-A::TeTxLC-tau-lacZ mice. BrdU (100 mg/kg) was injected into DG-A::TeTxLC-tau-lacZ and WT litters from P15 to P22 (8 days total) to label newly generated neurons in the DG. Horizontal brain sections from P23 animals were stained for BrdU (green) and DAPI (blue).
(I and J) Doublecortin (DCX) staining of DG sections from P23 WT, DG-S::TeTxLC-tau-lacZ and DG-A::TeTxLC-tau-lacZ mice. Nuclei were stained with DAPI (blue). (J) Quantification of the DCX staining intensity in the GCL. Data are shown as percentage of WT. Bars are mean ± SEM. 4 mice were analyzed in each group.
Scale bars are 50 μm.
See also Figure S4.

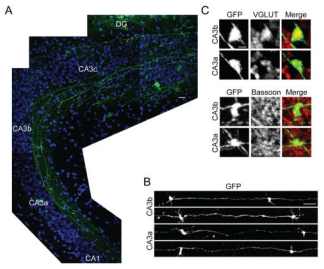

Figure 7. Dentate Granule Cells Born at P15 Send Axons and Form Synapses in CA3 by P23

(A) GFP-expressing retrovirus was injected into the DG of WT mice to label DGC progenitors at P15, and horizontal sections of the hippocampus were prepared at P23. GFP-positive mossy fibers with numerous large boutons extend to the CA3-CA1/2 border.

(B) Representative large boutons of GFP-positive mossy fibers. Boutons in the CA3a (distal) and CA3b (medial) areas are shown. In both areas, many morphologically mature large synaptic boutons are observed.

(C) GFP-positive mossy fiber boutons colocalize with presynaptic markers, VGLUT1 and bassoon.

Scale bars are 20 μm (A), 10 μm (B), and 2 μm (C).

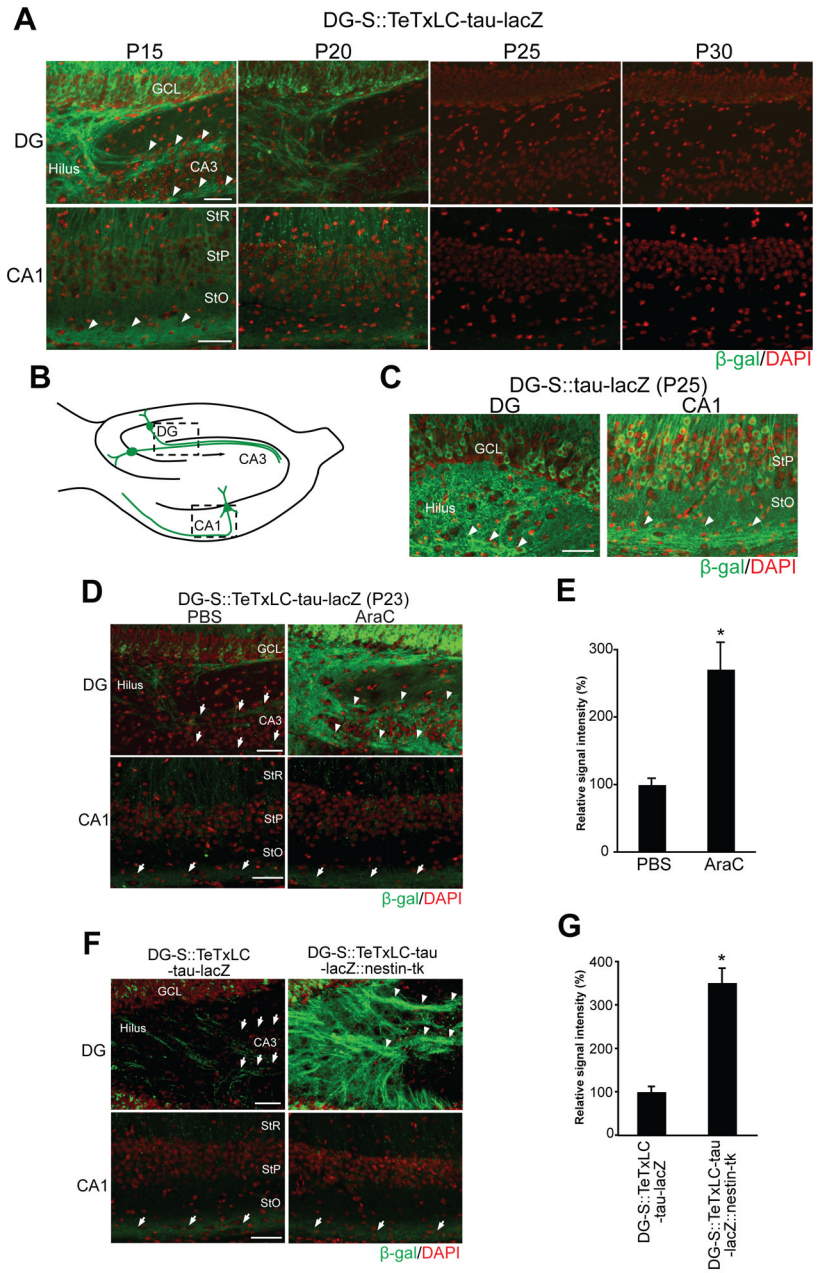

Figure 8. Suppression of Neurogenesis Inhibits the Elimination of Inactive DG Axons, but Not that of Inactive CA1 Axons, in Mice in which Some Mature DG and CA1 Neurons Are Inactivated

(A) Developmental elimination of inactive DG and CA1 axons in DG-S::TeTxLC-tau-lacZ mice (P15–P30), in which tTA/TeTxLC are expressed by a moderate number of mature DG and CA1 neurons. Horizontal hippocampal sections of DG-S::TeTxLC-tau-lacZ mice were stained with the anti-β-gal antibody (green). Nuclei were stained with DAPI (red). Pictured areas correspond to the boxed areas in (B). At P15, inactive DG and CA1 axons were present (arrowheads) in the hippocampus, but they were markedly reduced by P25 in both DG and CA1 regions. GCL, granule cell layer; StR, stratum radiatum; StP, stratum pyramidale; StO, stratum oriens.

(B) Schematic illustration of the hippocampus indicating pictured areas (DG and CA1) in (A), (C), (D), and (F).
(C) Immunostaining of the hippocampus of P25 DG-S::tau-lacZ mice with the anti-β-gal antibody (green). Active axons were maintained in both the DG and CA1 at P25. Arrowheads indicate β-gal positive axons.
(D and E) DG-S::TeTxLC-tau-lacZ mice were injected with PBS or AraC from P15 to P22 (8 days total) and their hippocampi were stained for β-gal (green) at P23. (D) In PBS-injected mice, inactive axons were eliminated in both DG and CA1 areas. In AraC-injected mice, inactive axons were maintained in the DG (arrowheads) but not in CA1. Arrows indicate the location of axons. (E) Quantification of the β-gal staining intensity in P23 PBS- or AraC-injected DG of DG-S::TeTxLC-tau-lacZ mice. Data are shown as percentage of PBS control. Bars are mean ± SEM; 9 mice for each condition. Differs from the PBS-injected mice at *p=0.018 by Student's t-test.
(F and G) DG-S::TeTxLC-tau-lacZ mice were mated with nestin-tk transgenic mice (DG-S::TeTxLC-tau-lacZ::nestin-tk). DG-S::TeTxLC-tau-lacZ::nestin-tk mice were injected with ganciclovir to suppress neurogenesis (P15 to P22). DG-S::TeTxLC-tau-lacZ mice (control) also received ganciclovir. Sections from P23 brains were stained for β-gal to visualize TeTxLC-expressing inactive axons (green). (F) In DG-S::TeTxLC-tau-lacZ mice, inactive axons were eliminated in both DG and CA1 areas. In contrast, in DG-S::TeTxLC-tau-lacZ::nestin-tk mice, inactive axons were maintained in the DG (arrowheads), but not in CA1. (G) Quantification of the β-gal staining intensity in the DG of P23 DG-S::TeTxLC-tau-lacZ and DG-S::TeTxLC-tau-lacZ::nestin-tk mice. Data are shown as percentage of DG-S::TeTxLC-tau-lacZ. Bars are mean ± SEM; 4 mice for each genotype. Differs from the DG-S::TeTxLC-tau-lacZ mice at *p<0.001 by Student's t-test. Scale bars are 50 μm.
See also Figure S5.